Proceedings of the Institute of Acoustics

# MEASUREMENT OF METEOROLOGICAL PARAMETERS OF THE ATMOSPHERIC BOUNDARY LAYER BY TOMOGRAPHIC SOUNDING

Detlef Englich, Volker Mellert, Ulrich Radek, Rainer Schmidetzki

University of Oldenburg,Germany

## 1. INTRODUCTION

Sound propagation outdoors is mainly influenced by the wind and temperature field determining the acoustic index of refraction. Measurement of sound propagation allows for the determination of the field of the refraction index by inverting the problem. This technique is well known in tomopraphic procedures, which are for instance applied in medical diagnosis.

The use of tomographic methods in environmental research is commonly applied in ocean acoustics [1]: Three dimensional pictures of the velocity and temperature field are reconstructed from long distances sound velocity measurements in water. The solution of the inverse problem can be achieved because assumptions on the wave propagation through the medium are made, which can be treated mathematically. Progress in understanding the sound propagation in the atmospheric boundary layer enables for reconstruction of temperature and wind profiles [2] as well as first statistical moments of the temperature and wind field [3, 4]. This paper reports measuring and evaluation techniques for determination of meteorological parameters from sound propagation measurements.

It is advantageous to use sound as a remote sensing tool for local meteo parameters because of the mobility of the measuring system compared to huge meteorological masts. The acoustic systems can be used in situations where it is difficult to mount a mast, e.g. near airfields. Micrometeorological problems, like the investigation of wakes behind windturbines or buildings, can be studied without using groups of individual sensor masts.

One important improvement of acoustical sounding compared to optical sensing is the increase in sensitivity. The index of refraction influences the acoustic wave in air about 104 times more than an electromagnetic (optic) wave. Therefore, the acoustic wave generally travels on a curved path through the atmosphere, which on the other hand makes the measuring system more complicated than for a straight forward radiation of electromagnetic waves used in known tomography.

## 2. RAY TRACING

The wave propagation can be traced on rays as long as the acoustic wavenumber is large compared to gradients of the field of the refraction index. This situation is often the case in the stratified boundary layer (except in direct vicinity of the ground). An index of refraction increasing with height causes sound rays to be bent downwards. Under downwind condition the sound waves radiated from a source can thus be measured with microphones near the ground. Simple and fast ray tracing procedures are available to simulate the sound propagation (e.g. [5, 6, 7]). Comparing the simulation with the measured magnitude and phase of the sound pressure at different distances from the source, it is possible to deduce the average wind and temperature field for numerous meteorological situations. In tomography, a sufficiently large number of propagation paths must be known to calculate the spatial distribution of the field of the refraction index. Since the function of the profile of the refraction index near the ground is known for some cases from meteorological boundary layer theory, a few different sound rays can already reveal the profile's parameters [2, 13]. Characteristic patterns of the ray propagation can be evaluated to determine specific parameters of the profile, even in cases of insufficient analytical description of the profile function.

## 3. WAVE PROPAGATION

A general analytical solution for the description of wave propagation through the inhomogenous, turbulent atmosphere does not exist. Numerical attempts to solve the wave equation with the assumption of frozen turbulence are successful, especially in using the concept of decomposing the refraction index profile in a Fourier series (Fast Field Program FFP [8]). But the numerical integration also bears some disadvantage: It is difficult to control the reliability. Increasing the resolution in space and frequency leads to extremely time consuming calculation. Solving the basic differential equation as far as possible with certain approximations reduces computation time, the numerical evaluation of the remaining integrals is usually much more efficient [9] than grid-wise integration of the wave equation.

It is practically hopeless to use the FFP approach for numerical determination of the statistics of the (non-frozen) atmosphere, though sometimes spare computer time might allow for the necessary large number of iterations [10]. Encouraging results have been achieved in developing methods for solving momentum equations [3, 4, 11]. Thus, it is possible to determine moments of the refraction index distribution from measured moments of the acoustic wave. This approach is principally outlined in [4] and has not been applied to the outside atmosphere yet, hence this paper just cites sample measurements carried out in a model atmosphere [18].

In the following, the main attention is directed to the use of ray tracing for tomographic sensing, though recently [9] the more sophisticated wave theory approach has principally been outlined, but not applied yet. The ray tracing algorithm used is based on the equations given in [7].

## 4. RAYS IN TYPICAL METEOROLOGICAL CONDITIONS

The interrelated wind and temperature functions in the boundary layer can be described by the Monin-Obukhov similarity theory [12], except for weak wind or in calm atmosphere. The friction velocity $u_*$ and the scaling temperature $T_*$ are combined in a stability parameter $L$ (Monin-Obukhov length):

$$L = \left(\frac{T_m}{g\kappa}\right)\frac{u_*^2}{T_*}, \tag{1}$$

with $T_m$: mean surface temperature; $g$: gravitational acceleration; $\kappa$: von Kármán constant ($\approx 0.41$);

$$u_* = \sqrt{< u'w' >} \;;\; T_* = \frac{< w'T' >}{u_*}, \tag{2}$$

with $u'$: horisontal wind speed fluctuation; $w'$: vertical wind speed fluctuation; $< \cdots >$ denotes time average. Empirical analytical expressions for wind and temperature profiles are given in [17]. In general, for $L > 0$ the stratification is stable and for $L < 0$ it is unstable.

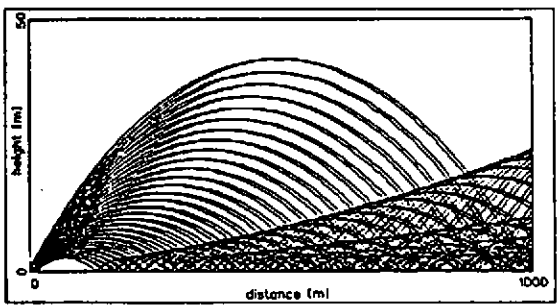


Figure 1: Typical picture of acoustical ray tracing for a choice of launching angles, calculated for stable meteorological conditions with a friction velocity $u_* = 0.2\,m/s$ and a temperature scaling factor $T_* = 0.1\,K$ corresponding to an Obukhov length of 30 m.

**Stable atmosphere**

(Horisontal) wind velocity $u$ and temperature $T$ are increasing with height $z$, the sound speed gradient $\nabla c$ ('gradient' refers to the horisontal vector component of the velocity) is positive. The sound rays are bent towards the ground and converge, the density of rays and hence the sound pressure levels increase near ground with increasing $\nabla c$, yielding the known enhancement of immission levels under downwind condition. A typical example is shown in figure 1. The curved rays are characterized by a maximal height $z_c$ and a typical distance $x_c$ between successive ground reflections. Both quantities are related to the profile parameters.

**Unstable atmosphere**

$T$ is decreasing and $u$ is increasing with height, the gradient $\nabla u$ rapidly decreases with height. Near the ground, the wind determines $\nabla c$, downwind ray patterns look similar to the stable atmosphere case. In larger heights, the ray pattern is determined by $\nabla T$. The rays are bent upwards and diverge, the sound pressure level is reduced [15]. A typical example is shown in figure 2. The neutral atmophere case lying between stable and unstable is characterised by a large magnitude of $L$; for details see e.g. [17].

**Low level jet**

Frequently, a low level jet occurs above a stable atmosphere. In this horisontal jet the wind is stronger and generally blows into a different direction than the surface wind. Rays penetrating into the low level jet may be focussed, as shown in figure 3. The horisontal distance between such a focus area and the sound source depends on the thickness of the surface layer and on the increase of $\nabla c$ in the low level jet. Increase in height or decrease of gradient causes focussing at larger distance [16].

**Profile similarities**

In a stable atmosphere $T(z)$ and $u(z)$ yield an approximatively logarithmic sound speed profile with a linear component $c_l z$ [5]:

$$c(z) = c_0 + c_* \, ln\left[\frac{(z+z_0)}{z_0}\right] + c_l z \tag{3}$$

with $z_0$: roughness length; $c_0 = c(z=0)$; and the linear scaling velocity component

$$c_l = u_l + 0.601\, T_l; \tag{4}$$

with $u_l$, $T_l$: linear components of $u(z)$ and $T(z)$; the scaling velocity

$$c_* = \frac{u_*}{\kappa} + 0.601\,\frac{T_*}{\kappa} \tag{5}$$

(for simplicity: wind velocity vector is parallel to sound propagation). A similarity relation holds for rays in

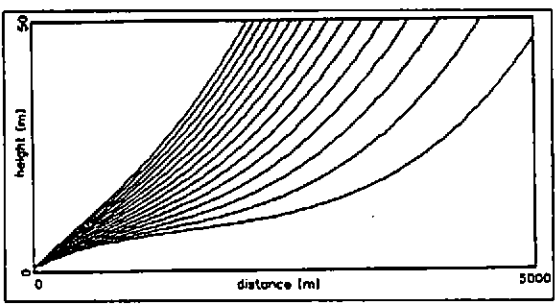


Figure 2: Picture like figure 1 for unstable conditions with $u_* = 0.15\,\mathrm{m/s}$ and $T_* = -0.4\,\mathrm{K}$ corresponding to an Obukhov length of $L = -4\,\mathrm{m}$. Note the different abszissa scale.

stable profiles [5]. The characteristic distance $x_c$ and the maximal height $z_c$ of each ray are related by

$$x_c = 2\left[\frac{c_t}{(2c_0 z_c)} + H\frac{c_*}{(c_0 z_0^2)}\right]^{-\frac{1}{2}} \tag{6}$$

with the empirical constant $H \approx 0.62$.

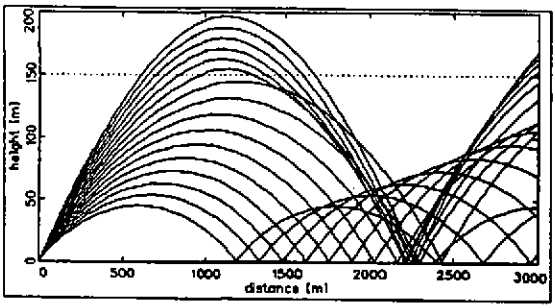


Figure 3: A low level jet frequently appears above a stable atmosphere. In this ray tracing simulation the stable atmosphere with $u_* = 0.3\,\mathrm{m/s}$ and $T_* = 0.1\,\mathrm{K}$ reaches up to 150 m. The low level jet is calculated with a linear vertical wind gradient of $0.12\,\mathrm{s}^{-1}$ from 150 m to 200 m. The data are based on measurements [14].

## 5. OBSERVABLES IN RAY HISTORY

The direct ray is the first one to arrive at the receiver, followed by rays, which are once or multiply reflected at the ground. These rays are phase lagged due to larger travel time, to increasing number of reflections (the amount of phase shift for every reflection, between 0 and $-\pi$, depending on the ground impedance $\varsigma$) and by grazing caustics (each contributing $-\pi/2$). It is possible to assign each ray a complete history of phase shifts undergone, coded in well defined regularity, as has been found empirically [5].

The angle of incidence of each ray depends on the sound velocity $c_t$ at the turning point (largest height reached) [19], this is simply a result of the law of refraction. The direct rays from source to two microphones, mounted a horizontal distance $d$ apart each other, arrive with a time difference $\Delta t_d$. Measuring $\Delta t_d$ yields $c_t$ according to the refraction law:

$$c_t = \frac{d}{\Delta t_d}. \tag{7}$$

The time difference $\Delta t_t$ between direct and once ground reflected ray is directly related to the scaling velocity $c_*$ in stable profiles [2]. It is given by $\Delta t_t = \Delta t' + \Delta t_g$ with $\Delta t_g$: geometrical time difference (without any profile); $\Delta t'$: additional time difference due to the profile. For a merely logarithmic profile the calculation yields [2]

$$u_* = \frac{\Delta t' \kappa c_0^2}{D} \tag{8}$$

with $D$: horizontal distance between source and receiver at same height. In stable conditions, two measurements of $\Delta t'$ are necessary at two heights $z_1$ and $z_2$, yielding [2]

$$L = 2.5\left(\frac{z_1\Delta t_2' - z_2\Delta t_1'}{\Delta t_1' - \Delta t_2'}\right), \tag{9}$$

$$c_* = \frac{\Delta t_1' c_0^2}{|D(1 + \frac{2.5 z_1}{L})|}. \tag{10}$$

Hence, profile parameters can be determined from time measurements of single rays. Using short impulses for acoustical measurements, these single rays can be identified. The impuls response at the receiver consists of a series of pulses, each one corresponding to a single ray path, and can be evaluated as long as the single pulses can be separated. In terms of wave theory [9], modes of the transmission, which add in phase at the receiver, are interpreted as rays.

## 6. MEASUREMENTS

Mesurement techniques based on eqs. (8,9,10) require an acoustic impulse of moderate power for distances of some hundred meters. An 'average' profile is determined by the measurement, "instantaneous" in time (because the speed of sound is large compared to the fluctuations in the atmosphere) and averaged in space. Results are reported in [2], details are omitted here. In the following, long distance propagation measurements are described, carried out with a powerful plasma impulse sound source [20]. A typical time signal in 1350 m distance is shown in figure 4a. Obviously a direct ray and one reflection are identifiable. Since profile parameters were monitored during the acoustic measurement with common meteorological equipment, a ray tracing simulation can be obtained (figure 4b) for comparison. The rays can be regarded as being grouped in bundles. Each bundle consists of rays hitting the microphone directly and rays ground-reflected just in front of the microphone, thus having a small time lag $\tau$. Part of the ray history is listed in table 1. Each bundle has its own group velocity and hence gives an impulse response with identifiable pulses in the sense of geometrical acoustics.

| launching angle [°] | arrival time difference [ms] | level decrease [dB] |
|---|---|---|
| 7.0410 | 0 | -38.7 |
| 7.0242 | 0.7 | -37.7 |
| 6.4875 | 4.6 | -40.4 |
| 6.4747 | 5.3 | -40.6 |
| 6.3033 | 7.3 | -45.5 |
| 6.2957 | 8.0 | -42.1 |
| 6.2277 | 9.6 | -46.1 |
| 6.2240 | 10.8 | -46.0 |

Table 1: Listing of the first four bundles of eigenrays shown in figure 4b. Launching angles, time differences between arrival of the individual rays and direct ray and level attenuation of the single rays are noted. The latter is calculated with the ray tube method using the cross-sectional area of the tube in a distance of 1 m to the source as reference [21].

Knowing geometrical data and atmospheric absorption, the shape (or spectrum) of the measuring impulse at the receiver can be calculated (figure 4c). The small reflection after 5 ms stems from a reflection at the source, it is therefore part of the sensing impuls.
Numerical superposition of the direct impulse with the ground reflected one of the same bundle yields the shape in figure 4d, taking into account a soft ground impedance $\zeta$ and the time lag $\tau$. The synthesised impuls resembles the measured one (figure 4a) quite well.
The second impulse in figure 4a stems from the bundle of rays being ground-reflected at half distance. The time difference between first and second bundle's impulse is according to the prediction of table 1. The geometric convergence of each bundle yields the level enhancement of the measured impulse (figure 4a) compared to the calculated one (figure 4d), assuming spherical spreading only. The level difference is of expected order. Since further peaks in the impulse response are predicted to be smaller (table 1), it is not possible to evaluate this part of the measured signal. Obviously these peaks disappear in the background noise.
Determination of the sound speed profile with eq. 7 needs the measurement of $\Delta t_d$ with at least two microphones. No time resolution of the impulse response itself is necessary. A measured example with a 500 Hz sine impulse of 150 ms duration is shown in figure 5. The impulse was radiated with an exponential horn (135 dB SPL at 1 m) and received by two microphones (d = 30 m) in a distance of 5.3 km from the source

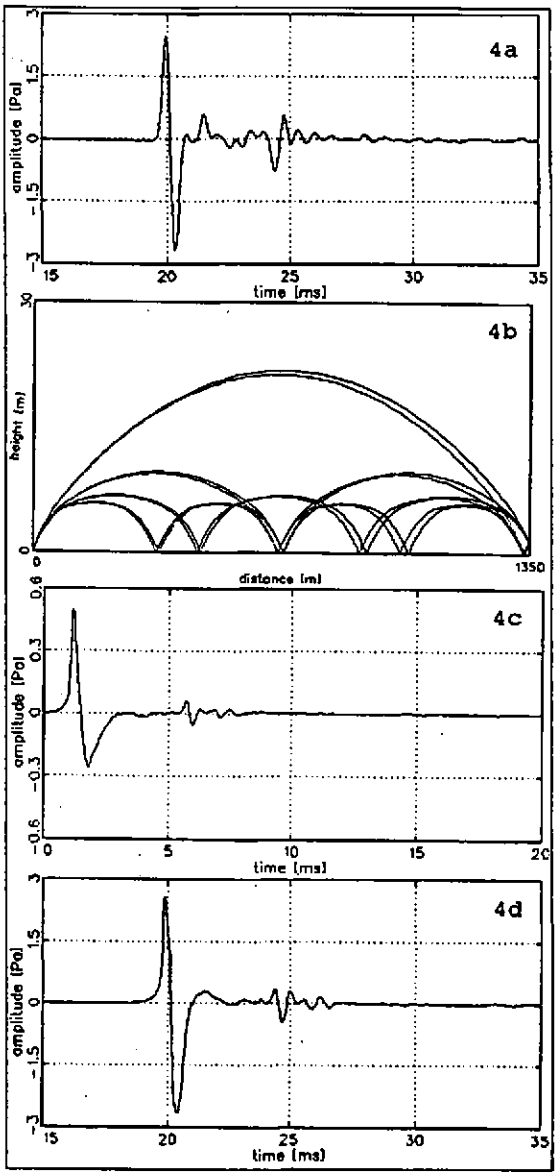


Figure 4: 4a shows a typical measured impulse time signal. The distance between source and receiver is 1350 m, the source is at the ground and the receiver at a height of 1.5 m. The peak to peak pressure amounts 5.7 Pa. Fig. 4b shows the corresponding ray tracing picture with the eigen rays, which hit the receiver. They were calculated with the meteorological data monitored during the measurement with a meteorological mast. The impulse at 20 ms in fig. 4a consist of the first ray bundle (tab. 1) with the direct ray and its reflection. Fig. 4c shows an impulse monitored near the source, corrected for the distance of 1350 m with respect to spherical spreading and atmospheric absorption (ISO 9613). This calculated impulse is used to construct an impulse similar to that in fig. 4a: Two impulses are added with the time difference within the first bundle of rays according to ray tracing. The phase of the second impulse is shifted 140° assuming a complex ground impedance. The result is drawn in fig. 4d.

[16]. Fig. 5a and figure 5b show typical microphone signals. Calculation of the instant phase between the two signals (figure 5c) yields a constant phase shift during the leading part of the signal (corresponing to the direct ray), which can be evaluated for $c_t$. With eqs. 3 and 6 it is possible to calculate the height of the turning point.

Two difficulties arise in this measuring technique: $\Delta t_d$ is unknown in multiples of the period of the sinusoidal test tone. By using three microphones or spectral broadening, the result will get unique. More problems arise from the meteorological conditions in the ground near surface layer, they are not reported in this paper.

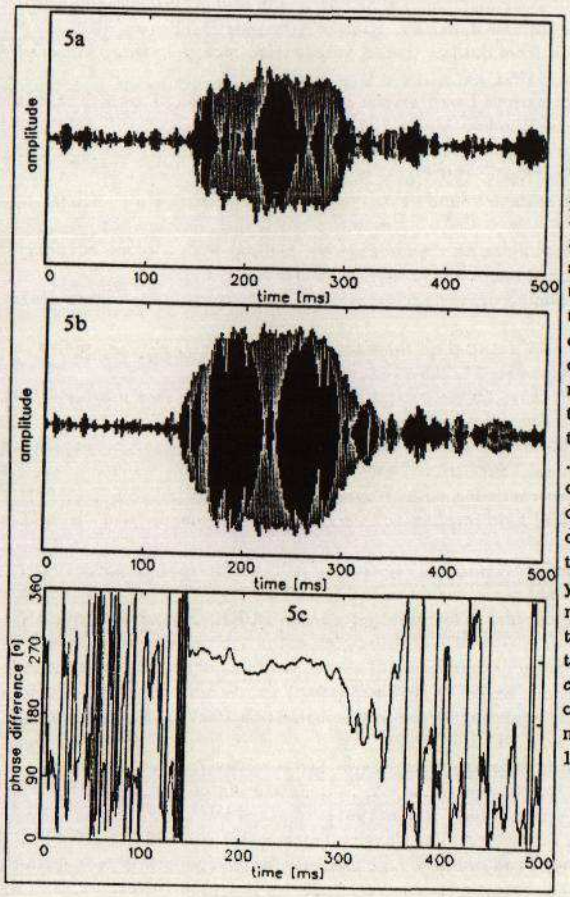


Figure 5: 5a and 5b show a 500 Hz sine pulse received by two microphones in 5.3 km distance from the source and 30 m apart each other. The time axis in 5b is shifted $\Delta t_{ref} = 87.4$ ms corresponding to the expected difference in arrival times for the sound velocity 343.2 m/s in the height of the microphones. 5c shows the phase difference between both time signals. It is nearly constant 270° in the range of the time signals. This difference corresponds to a time of 1.5 ms (or 3.5 ms, 5.5 ms ..., respectively, because of the periodicity of the signal). The difference 1.5 ms determines a time lag $\Delta t_d = 85.9$ ms, yielding a sound speed $c_t = 349$ m/s in the turning point. The time differences also yield the angle of incidence of the assumed plane wave fronts, which is calculated to 10.6°. A time difference of 3.5 ms determines a $\Delta t_d = 84.4$ ms, a sound speed $c_t = 355$ m/s and an angle of 15°. Both cases agree with results of ray tracing simulations (16° for the direct bundle and 11° for the second one).

*TOMOGRAPHIC SOUNDING IN THE ATMOSPHERE*

## 8. SUMMARY

Concepts of determining the sound speed profile in the atmospheric boundary layer through measurements of sound propagation are presented. Extraction of apropriate acoustic parameters and comparision with ray tracing simulations enables for a measurement of wind and temperature fields in the atmospere, future use of microphone arrays in special geometries will allow for an extended application to turbulence parameters and further approach the aim of tomographic sounding.

[1] *R.A. Knox: Ocean acoustic tomography: A primer. In: D.L.T. Anderson and J. Willebrand (Eds.), Oceanic circulation models: Combining data and dynamics.* Kluwer Academic Publishers, 1989.

[2] *H. Klug: Sound speed profiles determined from outdoor sound propagation measurements.* Accepted for publication in: J. Acoust. Soc. Amer., (1991)

[3] *R. Große: A local method of small pertubations based on the Helmholtz equation. Part I: The first statistical moment.* to appear in: Waves in Random Media 2 (1991)

[4] *R. Große and B. Li: Sound propagation in random media. A new theory generalizing the parabolic equation method.* Proc. Inst. of Acoustics, Keele, 1991.

[5] *W. Huisman: Analysis of ray patterns in realistic sound velocity profiles.* Doct.Diss., Univ. Nijmegen, The Netherlands, 1990.

[6] *M.M. Boone and E.A. Vermaas: Ray-tracing in an inhomogeneous medium with a plane boundary layer.* Proc. inter-noise 89, 313-316. Noise Control Foundation, New York, 1989

[7] *R.J. Thompson: Ray theory for an inhomogeneous moving medium.* J. Acoust. Soc. Amer., 51, 1675-1682 (1972)

[8] *S.J. Franke and G.W. Swenson Jr.: A brief tutorial on the Fast Field Program (FFP) as applied to sound propagagion in the air.* Applied Acoustics 27, 203-215 (1989)

[9] *I.P. Chunchuzov, G.A. Bush, S.N. Kulichkov: On acoustical impulse propagation in a moving inhomogeneous atmospheric layer.* J. Acoust. Soc. Amer. 88, 455-461 (1990)

[10] *H.E. Bass, W. McBride, J. Noble, R. Raspet: Effects of turbulence on outdoor sound propagation.* Proc. inter-noise 89, 367-372. Noise Control Foundation, New York, 1989

[11] *C.L. Rino: On propagation in continuous random media.* Waves in Random Media 2, 59-72 (1991)

[12] *A.S. Monin and A.M. Yaglom: Statistical fluid mechanics: Mechanics of turbulence.* Vol. 1. MIT, Cambridge, 1979

[13] *B. Hallberg, C. Larsson, and S. Israellson: Numerical ray tracing in the atmospheric surface layer.* J. Acoust. Soc. Amer. 83, 2059-2068 (1988)

[14] *H.Kraus, J.Malcher and E.Schaller: A nocturnal low level jet during PUKK.* Boundary-Layer Meteorol. 31, 187-195 (1985)

[15] *G.A. Daigle, T.F.W. Embleton, J.E. Piercy: Propagation of sound in the presence of gradients and turbulence near the ground.* J. Acoust. Soc. Amer. 79, 613-627 (1986)

[16] *D.Englich, H. Klug, U. Radek: Acoustic sounding of the atmospheric boundary layer (in German).* Fortschritte der Akustik, DAGA '90, Wien , 907-910 (1990).

[17] *A.J.Dyer: A review of flux profile relationships.* Boundary-Layer-Meteorology 7, 363-372 (1974)

[18] *R. Große, H. Lübbers, V. Mellert, M. Schultz-von Glahn, A. Sill: Scattering of sound by a random temperature field.* In preperation for J. Acoust. Soc. Amer.(1991)

[19] *D. Rind: Probing the atmosphere with infrasound.* The Physics Teacher, 2/1979, 102-108 (1979).

[20] *U. Radek, H. Klug, V. Mellert: Impulsive sound source of high intensity for outdoor sound propagation measurements.* Proc. 13th Int. Congr. on Acoustic (ICA), Vol. 2, 23-26, Belgrade 1989.

[21] *R.J. Thompson: Ray acoustic intensity in a moving medium (I+II)* J. Acoust. Soc. Amer. 55, 729-737 (1974)